energies

MDPI

Article

Lithium-Ion Battery Health State Prediction Based on VMD and DBO-SVR

Chunling Wu [1], Juncheng Fu [1,*], Xinrong Huang [1], Xianfeng Xu [1] and Jinhao Meng [2,*]

[1] School of Energy and Electrical Engineering, Chang'an University, Xi'an 710064, China; wuchl@chd.edu.cn (C.W.)
[2] School of Electrical Engineering, Xi'an Jiaotong University, Xi'an 710049, China
* Correspondence: 2021132007@chd.edu.cn (J.F.); jinhao@xjtu.edu.cn (J.M.)

Abstract: Accurate estimation of the state-of-health (SOH) of lithium-ion batteries is a crucial reference for energy management of battery packs for electric vehicles. It is of great significance in ensuring safe and reliable battery operation while reducing maintenance costs of the battery system. To eliminate the nonlinear effects caused by factors such as capacity regeneration on the SOH sequence of batteries and improve the prediction accuracy and stability of lithium-ion battery SOH, a prediction model based on Variational Modal Decomposition (VMD) and Dung Beetle Optimization -Support Vector Regression (DBO-SVR) is proposed. Firstly, the VMD algorithm is used to decompose the SOH sequence of lithium-ion batteries into a series of stationary mode components. Then, each mode component is treated as a separate subsequence and modeled and predicted directly using SVR. To address the problem of difficult parameter selection for SVR, the DBO algorithm is used to optimize the parameters of the SVR model before training. Finally, the predicted values of each subsequence are added and reconstructed to obtain the final SOH prediction. In order to verify the effectiveness of the proposed method, the VMD-DBO-SVR model was compared with SVR, Empirical Mode Decomposition-Support Vector Regression (EMD-SVR), and VMD-SVR methods for SOH prediction of batteries based on the NASA dataset. Experimental results show that the proposed model has higher prediction accuracy and fitting degree, with prediction errors all within 1% and better robustness.

Keywords: lithium-ion battery; state of health; variational mode decomposition; dung beetle optimization algorithm; support vector regression

Citation: Wu, C.; Fu, J.; Huang, X.; Xu, X.; Meng, J. Lithium-Ion Battery Health State Prediction Based on VMD and DBO-SVR. *Energies* **2023**, *16*, 3993. https://doi.org/10.3390/en16103993

Academic Editor: Djaffar Ould-Abdeslam

Received: 12 April 2023
Revised: 8 May 2023
Accepted: 8 May 2023
Published: 9 May 2023

1. Introduction

With the acceleration of economic globalization and the massive use of fossil fuels, environmental pollution and energy shortage have become increasingly prominent issues. Lithium-ion batteries for energy storage have found extensive applications across various facets of daily life and industrial production, owing to their substantial energy-storage capacity and excellent cycling performance [1]. With the growing number of applications for lithium-ion batteries, the battery will gradually age, leading to performance degradation. If used improperly, it may cause more serious accidents. Therefore, accurately and quickly estimating the SOH of the battery can provide necessary information for decision makers, enabling them to plan ahead, extend battery life, and enhance the safety of utilizing lithium-ion batteries. This has important practical significance [2]. Currently, although many methods exist for predicting the SOH, they are primarily categorized into two groups: model-based and data-driven approaches [3–6].

Equivalent circuit models or electrochemical models are the primary approaches utilized in model-based methods. Reference [7] proposed a method based on Electrochemical Impedance Spectroscopy (EIS) to estimate the SOH of lithium-ion batteries. Reference [8] estimated the SOH by constructing a nonlinear equivalent circuit battery model, where

the incremental state of charge (ΔSOC) is proportional to the SOH within a suitable voltage range. Reference [9] utilized the Forgetting Factor Recursive Least Squares (FFRLS) algorithm to identify the equivalent circuit model of Thevenin for battery parameters. In this model, the electrical resistance is used as the characteristic factor for battery health status and is estimated to determine the battery's SOH. The equivalent circuit model has a simple structure and low computational complexity, but its robustness is poor, and it is easy to produce estimation errors under different operating conditions. The electrochemical model establishes a dynamic system model based on the battery's electrochemical reaction mechanism and has higher accuracy, but it is difficult to identify parameters.

Data-driven methods essentially create a black-box model, where the internal structure of the battery does not need to be explicitly constructed. To construct a prediction model for SOH, it is only necessary to extract and analyze external parameters of the battery that are extremely correlated with SOH, and use them as training data. Reference [10] uses Convolutional Neural Network (CNN) to extract features and reduce data dimensionality of model input factors. Then, these factors are used as inputs of the Bidirectional Long and Short Term Memory (BiLSTM) network to predict the SOH. Compared with other neural networks, this approach provides higher prediction accuracy. Literature [11] proposed an SOH estimation method based on an improved Ant Lion Optimizer algorithm and Support Vector Regression (IALO-SVR). This method uses the IALO algorithm to optimize the kernel parameters of SVR, thereby improving the accuracy of SOH prediction. However, the accuracy of prediction results in the SVR model is directly affected by the penalty factor and kernel function parameters. Therefore, selecting appropriate model parameters is a critical issue that requires immediate attention when using the SVR method for estimating the SOH of lithium-ion batteries [12–14]. Literature [15] utilizes the Ensemble Empirical Mode Decomposition (EEMD) algorithm to decompose the original sequence signal into a trend signal and low-frequency residual signal in order to reduce the influence of various noises. Then, LSTM and CNN models are used to predict the SOH of the two types of signals separately. However, EEMD is prone to model mixing, which may affect the overall prediction accuracy.

To address the above issues, we extracted the available capacity of each charge-discharge cycle of the battery and calculated the corresponding SOH data. We used this SOH data as a health indicator and proposed a lithium-ion battery SOH prediction method based on the VMD-DBO-SVR model. Firstly, the VMD method is employed to decompose the original SOH sequence into a series of Intrinsic Mode Function (IMF) components that represent local features at multiple scales. Then, SVR is employed to model and predict each IMF element directly, and to address the difficulty in selecting SVR parameters, the DBO algorithm is utilized to optimize the parameters of the SVR model before model training. Finally, the predicted values of each sub-sequence are combined and reconstructed to derive the ultimate SOH prediction value. The proposed method is evaluated using the NASA dataset.

We compared the accuracy and practicality of our method with other methods using the same dataset in the literature. In reference [16], a Deep Neural Network (DNN) method was used to predict the SOH of lithium-ion batteries, which has better predictive performance compared to other machine learning models. However, due to the use of a single prediction model, the prediction accuracy is still not high enough. Reference [17] used a new physics-informed machine learning prediction model PIDDA, which includes three parts: autoencoder, physical information model training, and physics-based prediction adjustment, to achieve more accurate SOH prediction with less training data, but it did not consider the influence of dataset noise. Compared with the above two methods, our method considers the influence of noise and compensates for the problem of single model parameter selection, which has certain advantages. In summary, the main objective of this study is to eliminate the impact of battery capacity regeneration and various noises on capacity data, thereby eliminating the impact on SOH data, and solving the problem of difficult selection of SVR model parameters, thereby improving the accuracy of SOH prediction.

2. Basic Theory

2.1. Definition of Battery SOH

Battery SOH refers to the current health status of a battery, which is an important indicator of battery performance and service life, as the health status of a battery gradually deteriorates over time. SOH is typically expressed as a percentage and is defined as follows [18–20]:

$$\mathrm{SOH} = \frac{C_i}{C_0} \times 100\% \tag{1}$$

where, C_i is the available capacity of the i-th charge-discharge cycle, C_0 is the rated capacity.

2.2. VDM Decomposition

VMD is a variational method-based technique used to decompose nonlinear and non-stationary signals into multiple Intrinsic Mode Functions (IMF) [21,22]. The central concept of VMD is minimizing the interference among each IMF and other frequency bands through iterative optimization, which avoids information overlap and makes it robust to noise and interference. Since lithium-ion batteries are subject to capacity recovery and random interference during use, it is essential to employ VMD to remove noise interference. Here are the key stages of the algorithm:

Step 1: Construct the variational model. The original SOH signal is decomposed into K IMF, and the variational constraint function is formulated as follows:

$$\begin{gathered} \min_{\{u_k\},\{\omega_k\}} \left\{ \sum_{k=1}^{K} \left\| \partial_t \left[\left(\delta(t) + \frac{j}{\pi t} \right) * u_k(t) \right] e^{-j\omega_k t} \right\|_2^2 \right\} \\ \text{s.t.} \sum_{k=1}^{k} u_k(t) = f(t) \end{gathered} \tag{2}$$

where, $f(t)$ is the SOH data, $\{u_k\}$ is a set of K IMF components that have been decomposed, $\{\omega_k\}$ is a collection of central frequencies corresponding to each IMF component, $\delta(t)$ is the impulse function, $*$ is the convolution function.

Step 2: Introduce a penalty factor α and the Lagrange multiplier λ transforming a constrained variational problem into an unconstrained variational problem. The augmented Lagrange expression is derived as:

$$\begin{aligned} L = (\{u_k\},\{\omega_k\},\lambda) = \alpha \sum_{k=1}^{K} \left\| \partial_t [(\delta(t) + j/\pi t) * u_k(t)] e^{-j\omega_k t} \right\|_2^2 \\ + \left\| f(t) - \sum_{k=1}^{K} u_k(t) \right\|_2^2 + \left[\lambda(t), f(t) - \sum_{k=1}^{K} u_k(t) \right] \end{aligned} \tag{3}$$

Step 3: Initialize $\{u_k^1\}$, $\{\omega_k^1\}$, $\{\lambda^1\}$ and upper limit on the number of iterations n. In the Fourier transform domain, continuously iterate and update $\left\{\hat{u}_k^{n+1}\right\}$, $\left\{\omega_k^{n+1}\right\}$ and $\left\{\hat{\lambda}^{n+1}\right\}$. The update formula is as follows:

$$\hat{u}_k^{n+1}(\omega) = \frac{\hat{f}(\omega) - \sum_{i \neq k}^{K} \hat{u}_i(\omega) + \hat{\lambda}(\omega)/2}{1 + 2\alpha(\omega - \omega_k)^2} \tag{4}$$

$$\omega_k^{n+1} = \frac{\int_0^\infty \omega \left| \hat{u}_k^{n+1}(\omega) \right|^2 d\omega}{\int_0^\infty \left| \hat{u}_k^{n+1}(\omega) \right|^2 d\omega} \tag{5}$$

$$\hat{\lambda}^{n+1}(\omega) = \hat{\lambda}^n(\omega) + \gamma \left[\hat{f}(\omega) - \sum_{k=1}^{K} \hat{u}_k^{n+1}(\omega) \right] \tag{6}$$

where, γ is the noise tolerance; ω is the frequency.

Step 4: Stop the iterative updates until the stopping criteria are satisfied, which are as follows:

$$\sum_{k=1}^{K} \frac{\|\hat{u}_k^{n+1} - \hat{u}_k^n\|_2^2}{\|\hat{u}_k^n\|_2^2} < \varepsilon \tag{7}$$

where, ε is the discriminant accuracy, $\varepsilon > 0$.

2.3. Dung Beetle Optimization Algorithm (DBO)

The Dung Beetle Optimization (DBO) algorithm is a population-based intelligent optimization algorithm proposed by Jiankai Xue et al. [23], inspired by the rolling, dancing, foraging, stealing, and breeding behaviors of dung beetles. Specifically, the DBO algorithm achieves the traversal and search of the search space by simulating the behavior of dung beetles rolling dung balls. This algorithm also introduces some strategies, such as dance behavior to determine the direction of advancement, and grabbing behavior to jump out of local optimal solutions. The algorithm exhibits comparable competitiveness to the latest optimization strategies regarding the speed of convergence and accuracy of solutions.

The DBO algorithm mainly includes four types of behavior: rolling, breeding, foraging, and stealing, corresponding to four types of dung beetles: rolling dung beetle, breeding dung beetle, foraging dung beetle, and thief dung beetle. The algorithm achieves parameter optimization by having each type of dung beetle perform its corresponding operation. The specific four behaviors of the DBO algorithm are as follows:

(1) Rolling ball

The dung beetle rolls a much larger dung ball than itself and usually uses celestial cues such as the sun to navigate in order to maintain the dung ball's motion in a linear path. During the rolling process, the position of the rolling dung beetle is updated according to the following formula:

$$\begin{gathered} x_i(t+1) = x_i(t) + \alpha \times k \times x_i(t-1) + b \times \Delta x \\ \Delta x = |x_i(t) - X^w| \end{gathered} \tag{8}$$

where, t is the iteration count, $x_i(t)$ is the position information of the i-th beetle during the t-th iteration, $k \in (0, 0.2]$ is a fixed parameter representing the deviation factor, $b \in (0, 1)$ is a fixed parameter, α is the natural coefficient, which is allocated a value of either 1 or -1, X^w is the global worst position, Δx simulates the variation of light brightness.

When a dung beetle confronts an obstruction that blocks its path, it needs to reposition itself by dancing in order to find a new route. To simulate this dance behavior, a tangent function is used to obtain a new rolling direction. After the dung beetle determines a different direction, it continues to roll the ball backward. The position of the dung beetle is updated as follows:

$$x_i(t+1) = x_i(t) + \tan(\theta)|x_i(t) - x_i(t-1)| \tag{9}$$

where, θ is the deflection angle, which takes a value of $[0, \pi]$.

(2) Reproduction

In nature, female dung beetles roll their dung balls to a safe place suitable for laying eggs and hide them. Inspired by this behavior, a strategy for selecting boundaries is chosen to mimic the oviposition area of female dung beetles, which is defined as follows:

$$\begin{gathered} {L_b}^* = \max(X^* \times (1 - R), L_b) \\ {U_b}^* = \min(X^* \times (1 + R), U_b) \end{gathered} \tag{10}$$

where, X^* represents the current optimal position, ${L_b}^*$ and ${U_b}^*$, respectively, represent the lower and upper bounds of the oviposition area, $R = 1 - t/T_{max}$, T_{max} is the maximum number of iterations, L_b and U_b, respectively, represent the lower and upper bounds of the optimization problem.

Once the oviposition area is determined, the female beetle will select an egg in this area for laying. The boundary range of the oviposition area will dynamically change, which is mainly determined by the value of R, as can be clearly seen from Equation (10). Therefore, the position of the egg is also dynamic during the iteration process, defined as:

$$B_i(t+1) = X^* + b_1 \times (B_i(t) - Lb^*) + b_2 \times (B_i(t) - Ub^*) \tag{11}$$

where, $B_i(t)$ is the position of the i-th egg in the t-th iteration, b_1 and b_2 are two uncorrelated stochastic vectors of size $1 \times D$, D is the dimension of the optimization problem.

(3) Foraging

The eggs laid by female beetles will gradually grow. Some matured small beetles will come out of the ground to search for food. The optimal foraging area of small beetles is modeled as follows:

$$\begin{aligned} {L_b}^b &= \max\left(X^b \times (1-R), L_b\right) \\ {U_b}^b &= \min\left(X^b \times (1+R), U_b\right) \end{aligned} \tag{12}$$

where, X^b is the global optimal position, ${L_b}^b$ and ${U_b}^b$ represent the lower and upper bounds of the optimal foraging area. Therefore, the position update of the small dung beetles is as follows:

$$x_i(t+1) = x_i(t) + C_1 \times \left(x_i(t) - {L_b}^b\right) + C_2 \times \left(x_i(t) - {U_b}^b\right) \tag{13}$$

where, $x_i(t)$ represents the position of the i-th small dung beetle in the t-th iteration, C_1 represents a random variable that follows a normal distribution, C_2 is a random vector within the range of (0, 1).

(4) Stealing

There are some beetles, called thieves, that steal dung balls from other beetles. From Equation (12), it can be seen that X^b is the optimal food source, so it can be assumed that the area around X^b is the optimal location for competing food. During the iteration process, the position of the thief is updated as follows:

$$x_i(t+1) = X^b + S \times g \times \left(|x_i(t) - X^*| + \left|x_i(t) - X^b\right|\right) \tag{14}$$

where, $x_i(t)$ represents the position of the i-th thief at the t-th iteration, g is a random vector of size $1 \times D$ following a normal distribution, S is a constant.

2.4. Support Vector Regression (SVR)

The SVR method finds the best hyperplane that fits the data by continuously reducing the error between predicted and actual values. Its advantage is strong generalization ability and good performance in handling nonlinear problems [24,25].

Assuming a given sample set $S = \{x_i, y_i\}_{i=1}^n (x_i \in X = R^n, y_i \in Y = R)$. Where x_i is the i-th input vector, y_i is the corresponding output vector, and n is the total number of all samples. By utilizing the SVR method, non-linear mapping is applied to map the sample set from a low-dimensional space to a high-dimensional space. This non-linear mapping can be defined as:

$$f(x) = \omega \cdot \phi(x) + b \tag{15}$$

where, x, b, ω represent input data, intercept, and weights, respectively. Then introduce the slack variables $\{\xi_i\}_{i=1}^n$ and $\{\xi_i^*\}_{i=1}^n$, we can get:

$$\min R(\omega, b, \xi) = \frac{1}{2}\|\omega\|^2 + C\sum_i^n (\xi_i + \xi_i^*) \tag{16}$$

$$\text{s.t.} \begin{cases} y_i - \omega \cdot \phi(x) - b \leq \varepsilon + \xi_i \\ \omega \cdot \phi(x) + b - y_i \leq \varepsilon + \xi_i^* \\ \xi_i, \xi_i^* \geq 0. \end{cases} \tag{17}$$

where, C is the penalty factor, $\varepsilon(\varepsilon > 0)$ is the highest acceptable error of the regression. Introducing Lagrange multipliers and kernel function, Equation (16) can be converted into the following equation:

$$\max R(\alpha_i^*, \alpha_i) = -\frac{1}{2}\sum_{i,j}^{n}(\alpha_i^* - \alpha_i)\left(\alpha_j^* - \alpha_j\right)\phi(x_i)\phi\left(x_j\right) - \sum_{i}^{n}\alpha_i(y_i + \varepsilon) + \sum_{i}^{n}\alpha_i^*(y_i - \varepsilon) \tag{18}$$

Subject to:

$$\text{s.t.} \begin{cases} \sum_{i}^{n}(\alpha_i - \alpha_i^*) = 0, \\ 0 \leq \alpha_i, \alpha_i^* \leq C, \ \ i = 1, 2, \ldots n \end{cases} \tag{19}$$

where, α_i and α_i^* are Lagrange multipliers. After minimizing the Lagrangian function, the SVR expression for the non-linear mapping can be obtained. This expression can be formulated as:

$$f(x) = \sum_{i}^{n}(\alpha_i - \alpha_i^*)K(x_i, x) + b \tag{20}$$

where, $K(x_i, x) = \phi(x_i)\phi\left(x_j\right)$ is the kernel function. The Radial Basis Function (RBF) is a widely adopted nonlinear function and is also frequently used in SVR [26]. RBF can be defined as Equation (21).

$$K_{RBF}(x_i, x) = \exp\left(-\frac{1}{2\sigma^2}\|x_i - x\|^2\right) \tag{21}$$

where, σ is the kernel parameter.

3. SOH Prediction Based on VMD-DBO-SVR Combination Model

3.1. SVR Method Based on DBO Optimization

This paper employs the SVR method to establish the SOH prediction model. However, the selection of the penalty factor C and kernel parameter σ has a crucial impact on the forecasting precision of the SVR model. Larger C values and smaller σ values may lead to overfitting, while smaller C values and larger σ values may lead to underfitting. Due to the strong global optimization ability and fast convergence speed, as well as robustness, of the DBO algorithm, this paper uses the DBO algorithm to tune the penalty factor C and kernel parameter σ, aiming to improve the prediction accuracy of the SVR method.

The process of DBO for optimizing SVR parameters is illustrated in Figure 1, with the main procedures as follows:

(1) Initialization parameters for DBO algorithm: population size of dung beetles (pop), the proportion of four types of dung beetles in the population including rollers, breeders, foragers, and thieves, the dimension of variable parameters (dim), the maximum number of iterations (T_{max}), and lower bound (L_b) and upper bound (U_b).

(2) Randomly initialize the positions of all dung beetles.

(3) Calculate the fitness values of all dung beetles and record the global optimum position. In this study, the Mean Square Error (MSE) between actual and predicted values is applied to establish the fitness function, namely:

$$MSE = \frac{1}{n}\sum_{i}^{n}(\hat{y}_i - y_i)^2 \tag{22}$$

where, $\hat{y}_i$ is the i-th decomposition component of predicted SOH, y_i is the i-th decomposition component of actual SOH.

(4) Update the positions of all dung beetles: if it is a rolling dung beetle, update its position by rolling action according to Equation (8) in obstacle-free mode or by dancing action according to Equation (9) in obstacle mode; if it is a breeding dung beetle, update its position by breeding action according to Equations (10) and (11); if it is a foraging dung beetle, update its position by foraging action according to Equations (12) and (13); if it is a thief dung beetle, update its position by theft action according to Equation (14).

(5) After the update, determine if the position of each individual dung beetle exceeds the boundaries L_b and U_b. If it does, return to step (3). Otherwise, continue the execution.

(6) Update the present optimal solution and its fitness value.

(7) Repeat the above steps (3) to (6) until the iteration limit T_{max} is attained, and output the optimal parameters to the SVR model.

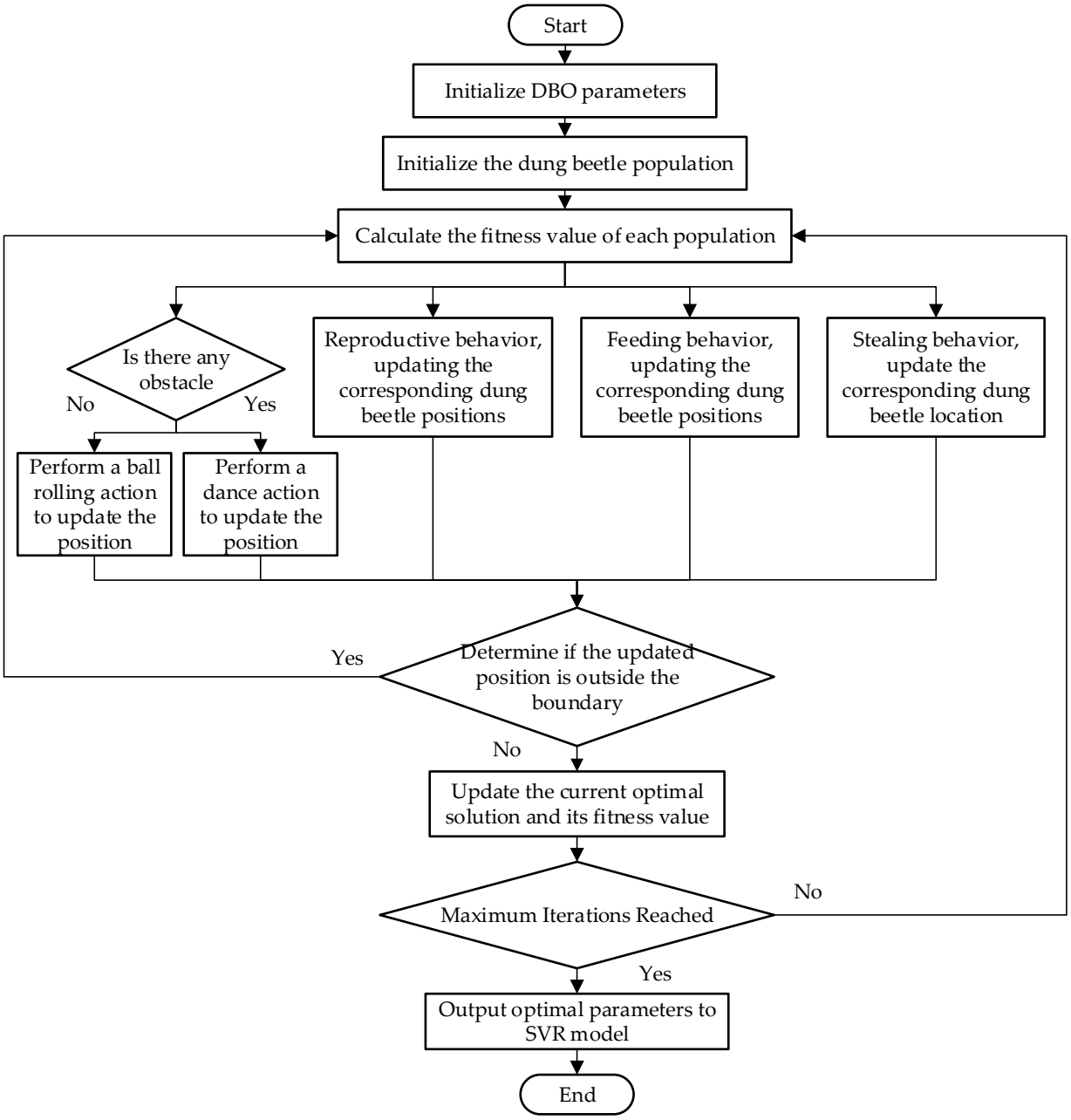

Figure 1. Optimization process of SVR parameters using DBO algorithm.

3.2. Combined Forecasting Model Framework Based on VMD-DBO-SVR

The flowchart of the combined prediction model based on VMD-DBO-SVR is illustrated in Figure 2.

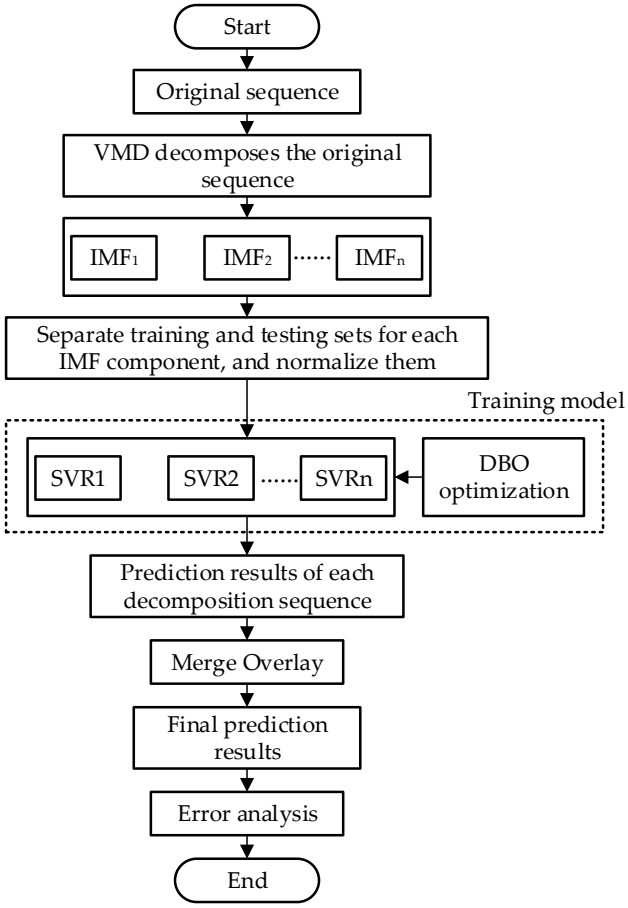

Figure 2. VMD-DBO-SVR forecasting model process.

The lithium-ion battery prediction model in this paper consists of four steps:

(1) Using VMD decomposition to decompose the original sequence of battery SOH into various modal components with different frequency bands.

(2) Preprocess the data of each mode component obtained by VMD decomposition, normalize it, and divide the preprocessed data into training data and testing data. Use the mode component data of the k-th iteration as input and the mode component data of the k + 1-th iteration as output.

(3) Build an SVR prediction model for each component separately and update the optimal SVR parameters using the DBO optimization algorithm.

(4) Validate the existing model with the test data, perform reverse normalization on the predicted values of each component, combine and superimpose the components, obtain the final SOH prediction result, and conduct error analysis.

4. Experimental Results and Comparative Analysis

4.1. Experimental Data and Parameter Settings

The dataset used in this experiment is from the Prognostics Center of Excellence (PCoE) at NASA. The dataset includes aging test data for three 18,650 lithium-ion batteries with a rated capacity of 2 Ah each, labeled B5, B6, and B7. All data were collected at a temperature of 24 °C using the CC-CV cycle test method for aging testing. Firstly, the battery is charged with a steady current of 1.5 A. When the battery voltage hits 4.2 V, the steady voltage mode is applied to continue charging the battery until the charging current

drops below 20 mA. Then, the battery is discharged at a steady current of 2 A until the voltages of B5, B6, and B7 drop to 2.7 V, 2.5 V, and 2.2 V, respectively. B5–B7 batteries have undergone 168 charge-discharge cycles, and the data includes measured voltage, current, temperature, and the available capacity for each cycle. Therefore, this dataset is mainly used for predicting the SOH and RUL, and estimating the State of Charge (SOC) of lithium-ion batteries. We extract the available capacity from each charge-discharge cycle and process it as SOH degradation data according to the SOH definition, enabling us to estimate the SOH of lithium-ion batteries. The detailed parameters of the 3 batteries are shown in Table 1, and the SOH degradation curves are shown in Figure 3.

Table 1. Detailed parameters of the experimental dataset.

Number	Temperature/°C	Discharge Current	Capacity/Ah	Shutdown Voltage/V
B5	24	2A/CC	2	2.7
B6	24	2A/CC	2	2.5
B7	24	2A/CC	2	2.2

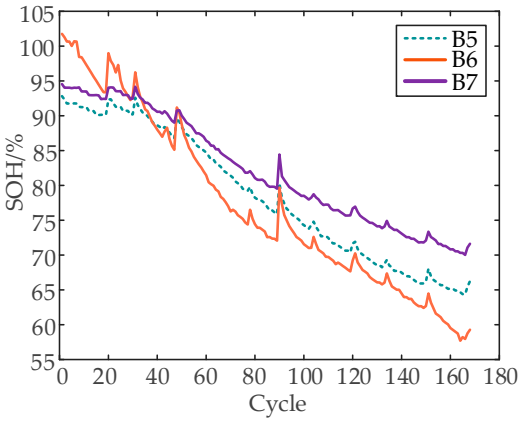

Figure 3. SOH degradation curves of NASA dataset battery B5, B6, and B7.

To more comprehensively demonstrate the adaptability of the VMD-DBO-SVR prediction method, in this experiment, 50% and 60% of the SOH data were, respectively, selected as the training set, and the remaining 50% and 40% of the data were applied as the test set to test the performance of the model.

When using the VMD algorithm for signal decomposition, it is necessary to select the mode number K beforehand. If the chosen number of modes is insufficient, certain significant information in the initial signal may be lost. On the other hand, if the selected mode number is too large, it may lead to frequency aliasing. Therefore, in this study, the mode number K is determined by examining the arrangement of center frequencies under various decomposition mode numbers. Taking the B5 battery as an example, the center frequencies under different K values are shown in Table 2.

Table 2. Center frequency of B5 battery under different K values.

K	Center Frequency/Hz					
2	1.97×10^{-5}	0.233	-	-	-	-
3	1.97×10^{-5}	0.166	0.328	-	-	-
4	1.96×10^{-5}	0.095	0.233	0.357	-	-
5	1.96×10^{-5}	0.093	0.167	0.292	0.401	-
6	1.96×10^{-5}	0.066	0.1664	0.224	0.330	0.402

As shown in Table 2, when K = 6, the central frequencies of the third and fourth mode components are close, indicating an over-decomposition phenomenon. Therefore, K = 5

is determined. The time-domain and corresponding frequency-domain plots of the SOH signal of battery B5 after VMD decomposition are shown in Figures 4 and 5, respectively.

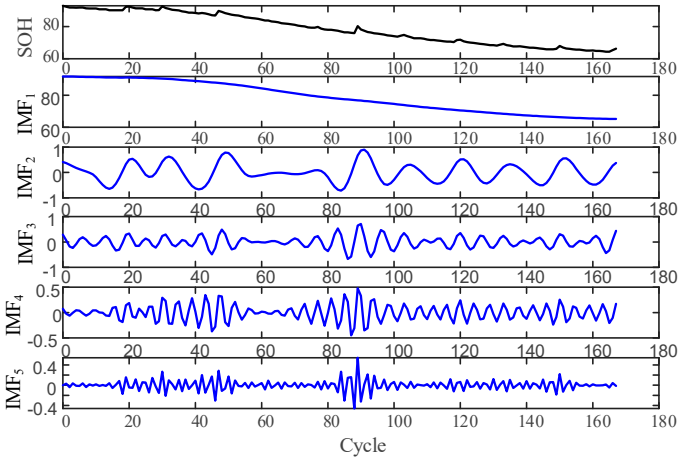

Figure 4. Time-domain diagram of VMD decomposition for B5 battery.

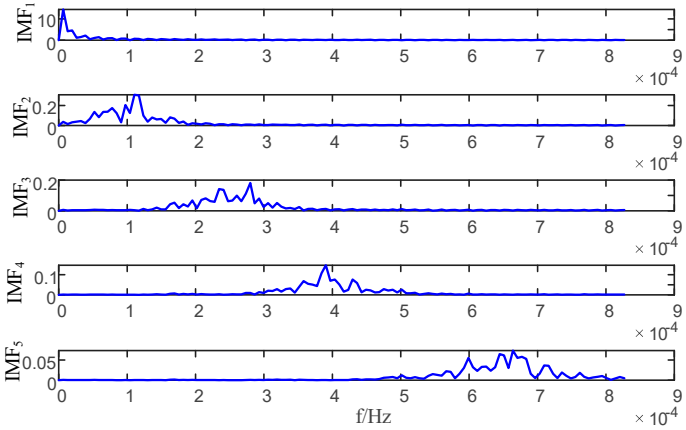

Figure 5. Spectrum diagram of B5 battery after VMD decomposition.

In Figure 4, IMF_1 represents the main trend of the original signal, IMF_2 and IMF_3 represent the periodic small fluctuations of the original signal within a shorter time period, and IMF_4 and IMF_5 represent the signal variations in the higher frequency band. Therefore, VMD can effectively decompose the different components of lithium battery SOH aging data. As shown in Figure 5, the mode mixing phenomenon of the original signal is well suppressed.

The parameter settings used in this paper for optimizing with the DBO algorithm are as follows: the number of dung beetle populations is pop = 30; the proportion of roller dung beetles, breeding dung beetles, foraging dung beetles, and thief dung beetles in the dung beetle population is 0.2, 0.2, 0.2, and 0.4, respectively; the dimension of variable parameters is dim = 2; the upper limit for the number of iterations is $T_{max} = 50$; the lower boundary is $L_b = 0.01$; and the upper boundary is $U_b = 100$.

4.2. Evaluation Index

(1) Mean Absolute Percentage Error (MAPE):

$$\mathrm{MAPE} = \frac{1}{n}\sum_{i}^{n}\left|\frac{\hat{y}_i - y_i}{y_i}\right| \times 100\% \tag{23}$$

(2) Root Mean Square Error (RMSE):

$$\mathrm{RMSE} = \sqrt{\frac{1}{n}\sum_{i}^{n}(\hat{y}_i - y_i)^2} \tag{24}$$

(3) Relative Accuracy (RA):

$$\mathrm{RA} = \frac{1}{n}\sum_{i}^{n}\left[1 - \left|\frac{\hat{y}_i - y_i}{y_i}\right|\right] \tag{25}$$

where, $\hat{y}_i$ is the predicted SOH; y_i is the actual SOH.

The performance of the proposed model is evaluated using the above indicators in this paper. A smaller value of MAPE and RMSE indicates a more accurate prediction result, while a value closer to 1 for RA demonstrates a better prediction performance of the model.

4.3. Experimental Verification and Analysis of SOH Prediction Based on VMD-DBO-SVR Model

When 60% of the data from three lithium-ion batteries were taken as the training set (B5, B6, and B7 with 100 cycles each), the fitting of the SOH prediction results based on the VMD-DBO-SVR model and the actual test results of the lithium-ion batteries are shown in Figure 6. The corresponding prediction errors are shown in Table 3, where ST represents the starting point of the prediction.

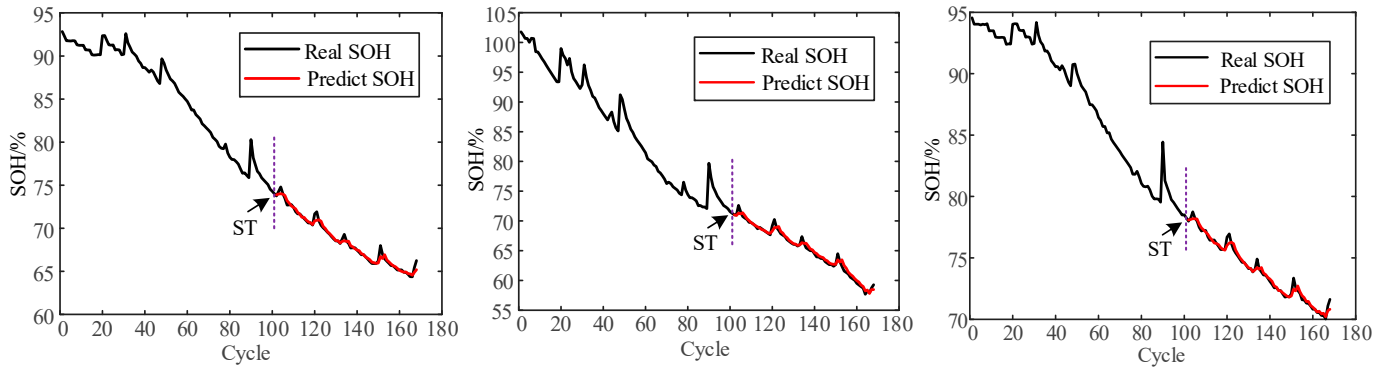

Figure 6. SOH prediction results with 60% data set of three batteries as training set. (**a**) B5; (**b**) B6; (**c**) B7.

Table 3. Prediction results of the VMD-DBO-SVR model based on the training dataset of 60%.

Battery	MAPE/%	RMSE	RA
B5	0.3511	0.3488	0.9964
B6	0.5863	0.5019	0.9941
B7	0.2594	0.2765	0.9974

As shown in Figure 6, the predicted SOH values for the three batteries are very close to the true values, indicating that the proposed method can effectively predict the trend of battery SOH and has good prediction accuracy. As shown in Table 3, the best prediction performance among the three batteries is B7, with an RA of 99.74% and RMSE and MAPE of 0.5019 and 0.2594%, respectively. The worst prediction performance is for B6, but its RA value is also as high as 99.41%, and RMSE and MAPE are only 0.2765 and 0.5863%, respectively. These results demonstrate that the VMD-DBO-SVR model proposed in this paper has good applicability to different lithium-ion batteries and can maintain high prediction accuracy.

To further verify the SOH prediction accuracy of the proposed model with insufficient training data, 50% of the data from three batteries were selected as the training set (B5, B6, and B7 with 84 cycles each), and the remaining 50% were used as the test set for SOH prediction. When 50% of the data was used for training, the fitting of the lithium-ion battery SOH prediction results based on the VMD-DBO-SVR model to the true test results is shown in Figure 7, and the corresponding prediction errors are shown in Table 4.

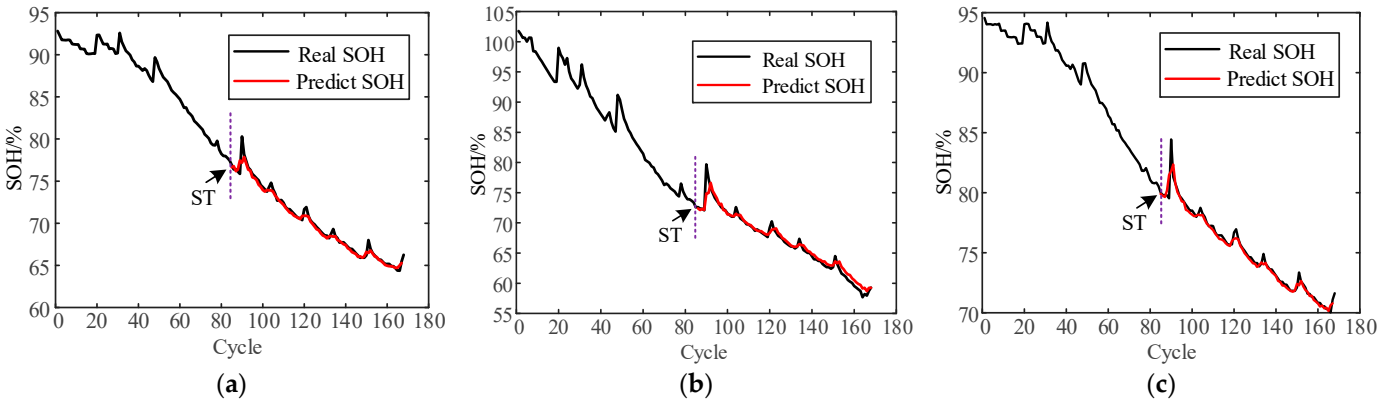

Figure 7. SOH prediction results of three batteries with 50% dataset as training set. (**a**) B5; (**b**) B6; (**c**) B7.

Table 4. Prediction results of the VMD-DBO-SVR model based on a 50% dataset as training set.

Battery	MAPE/%	RMSE	RA
B5	0.3906	0.4771	0.9961
B6	0.7892	0.8227	0.9921
B7	0.3318	0.4828	0.9966

When using fewer data as the training set, the prediction accuracy will decrease as shown in Figure 7, indicating that the less effective information provided during modeling from the early stage of prediction, the greater the error in the prediction results. However, the proposed model in this paper still has a good predictive effect. As shown in Table 4, even for battery B6 with the worst prediction accuracy, its RA value still reaches 99.21%, and the RMSE and MAPE values are only 0.8227 and 0.7892%, respectively. Compared with 60% training data, the corresponding RA value only decreases by 0.2%, while the RMSE and MAPE values increase by only 0.3227 and 0.2029%, respectively, indicating that the proposed prediction model has good generalization ability.

4.4. Comparative Analysis of VMD-DBO-SVR Model with Other Models

To validate the effectiveness and superiority of the VMD-DBO-SVR model proposed in this paper for predicting the SOH, three batteries were selected with 50% of their data employed as the training set, and compared with three other prediction models: SVR, EMD-SVR, and VMD-SVR. Figure 8 shows the comparison of the prediction results under different algorithms, and the corresponding prediction errors are shown in Table 5.

Figure 8 reveals that the single model SVR has the worst prediction performance, and its estimation error gradually increases in the later stage, indicating poor prediction accuracy. Although the EMD-SVR model reduces the error, the prediction accuracy is still poor and has not stabilized. The VMD-SVR model overcomes the end effect and modal aliasing phenomenon of EMD decomposition, and compared with the EMD-SVR model, the prediction performance is significantly improved, but the prediction accuracy is still not high enough. The VMD-DBO-SVR model proposed in this paper preprocesses the initial SOH data using the VMD decomposition method to reduce noise in the original data. After optimizing the SVR model parameters using the DBO algorithm, the prediction model is

trained to accurately predict the overall degradation trend of the battery and has good tracking ability for capacity regeneration, resulting in the best prediction performance.

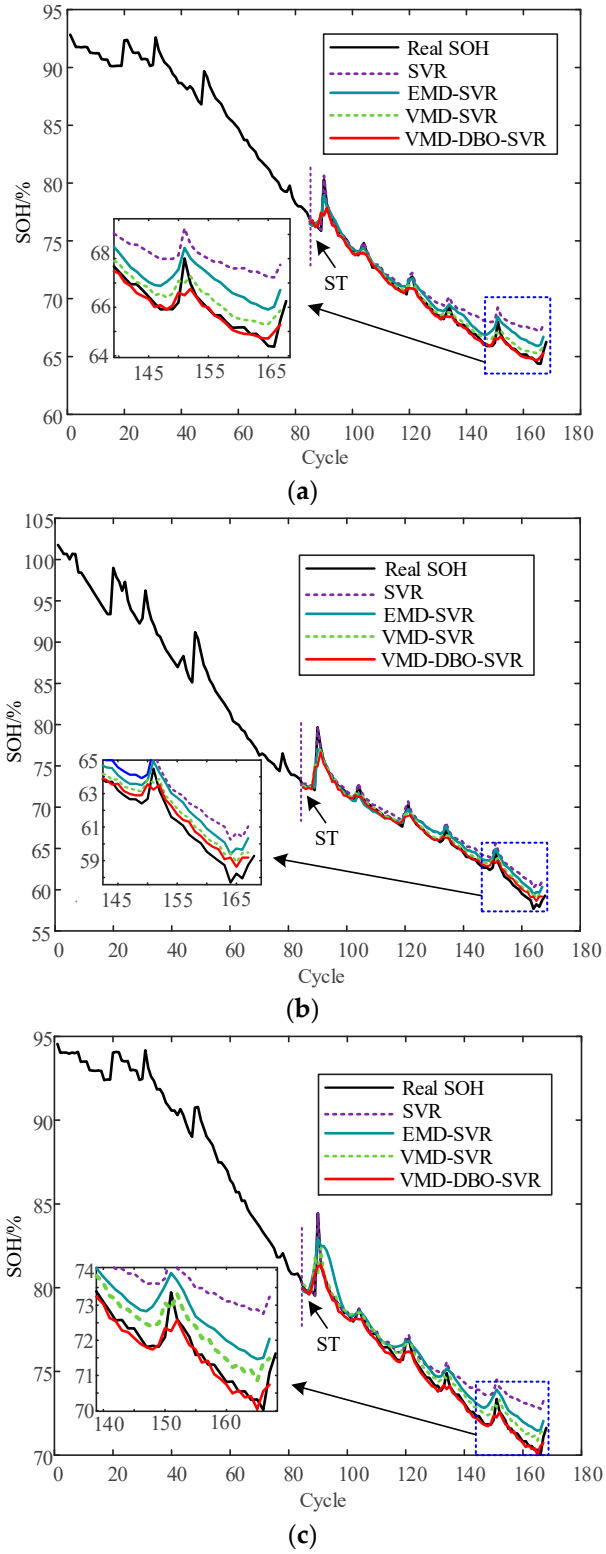

Figure 8. Comparison of SOH prediction results under different models for three batteries. (**a**) B5; (**b**) B6; (**c**) B7.

Table 5. SOH Prediction Errors of Different Models for three Batteries.

Battery	Model	MAPE/%	RMSE	RA	Prediction Time/s
B5	SVR	1.7833	1.5486	0.9821	0.6875
	EMD-SVR	1.1607	0.9775	0.9883	3.2114
	VMD-SVR	0.6467	0.5797	0.9935	3.4732
	VMD-DBO-SVR	0.3906	0.4771	0.9961	3.7297
B6	SVR	1.9822	1.6458	0.9801	0.7751
	EMD-SVR	1.3974	1.3233	0.9860	3.2046
	VMD-SVR	1.0090	0.9082	0.9899	3.6104
	VMD-DBO-SVR	0.7892	0.8148	0.9921	3.9867
B7	SVR	1.4489	1.4325	0.9855	0.6658
	EMD-SVR	1.1933	1.0556	0.9880	3.1699
	VMD-SVR	0.7364	0.6431	0.9926	3.1105
	VMD-DBO-SVR	0.3318	0.4828	0.9966	3.4405

From Table 5, it can be seen that the SVR model has a shorter prediction time, but its error is too large, which may result in unsatisfactory prediction results in practical applications. Compared with the EMD-SVR and VMD-SVR methods, the proposed model has a significant improvement in prediction accuracy with a relatively small increase in prediction time. Taking the B5 battery as an example, the RMSE of SVR, EMD-SVR, and VMD-SVR models are 1.5486, 0.9775, and 0.5797, and their prediction time are 0.6875 s, 3.2114 s, and 3.4732 s, respectively, while the RMSE and prediction time of the proposed model are 0.4771 and 3.7297 s, proving that the proposed model has higher accuracy than the other three models with only a small increase in prediction time.

To further demonstrate the superiority of the proposed VMD-DBO-SVR prediction method, still using battery B5 as an example and under the same initial conditions with the same training set, we compared the prediction results of our method with those of recently published models in related literature. The comparison results are shown in Table 6.

Table 6. Comparison of prediction results between proposed method and other method in literature.

Battery	Model	MAPE/%	RMSE
B5	IALO-SVR [11]	0.7400	0.6841
	ABMS-CEEMDAN-LSTM [27]	1.3145	1.0948
	VMD-DBO-SVR	0.3906	0.4771

From Table 6, it can be seen that although Reference [11] uses an improved ant lion optimizer to optimize the SVR parameters, it ignores the noise effect of the initial capacity data of batteries, resulting in lower prediction accuracy. Reference [27] reduces the impact of battery capacity regeneration by using an adaptive double exponential model smoothing method and denoising the lithium battery capacity data using CEEMDAN. However, the modal aliasing effect caused by CEEMDAN is unavoidable, resulting in inaccurate prediction. In general, the VMD-DBO-SVR model proposed in this work achieves higher prediction accuracy.

In this section, we first conducted simulations with 60% of the training data to validate the precision of the proposed method on three batteries. Then, we reduced the training data to 50% to demonstrate that the prediction accuracy decreases with the decrease of training data, but the proposed model still has good prediction performance. Furthermore, we compared the proposed model with SVR, EMD-SVR, and VMD-SVR models from prediction accuracy and running time, the experimental results showed that the proposed model had significantly improved prediction accuracy with a small increase in computation time. Finally, we compared the proposed model with relevant methods in recent literature to confirm its superior predictive performance.

5. Conclusions

Accurately predicting the SOH of lithium-ion batteries can improve their safety during operation and prevent accidents. We propose a SOH prediction model based on Variational Mode Decomposition (VMD) and Dung Beetle Optimization-Support Vector Regression (DBO-SVR). Through verification and analysis, the primary conclusions of this paper are as follows:

(1) The VMD algorithm can decompose the battery SOH sequence into multiple stationary mode components, which can effectively reduce noise interference, such as capacity regeneration and testing errors, and minimize prediction errors.
(2) The selection of kernel parameters in the SVR method directly affects the accuracy of SOH prediction. To address this issue, we proposed a DBO optimization algorithm to provide the optimal parameters for the SVR method. The combination of the two methods can improve the prediction accuracy and stability of SOH.
(3) NASA battery dataset was employed to validate the prediction performance of the proposed VMD-DBO-SVR model. The results showed that the VMD-DBO-SVR model had good prediction accuracy and stability, and the prediction error was maintained within 1%.

The above conclusion indicates that the model solves various noise interference problems through the VMD algorithm, and solves the problem of difficult SVR parameter selection through the DBO optimization algorithm, thereby improving prediction accuracy and achieving the preliminary research objectives of this article.

In actual SOH prediction for lithium-ion batteries, it is sometimes difficult to directly measure the available capacity of the battery, making the approach proposed in this paper unsuitable. Therefore, the next research direction of this paper is to use easily measurable feature factors that characterize the degradation pattern of SOH.

Author Contributions: Conceptualization, C.W. and J.F.; methodology, C.W. and J.F.; software, X.H. and X.X.; validation, J.M. and C.W.; formal analysis, J.M.; investigation, J.F.; resources, C.W. and X.H.; data curation, X.X.; writing—original draft preparation, C.W. and J.F.; writing—review and editing, C.W.; visualization, X.X.; supervision, J.F.; project administration, C.W.; funding acquisition, C.W. and X.H. All authors have read and agreed to the published version of the manuscript.

Funding: This research was funded by the National Key R&D Program of China and the Key R&D Plan of Shaanxi Province, grant number 2021YFB2601300 and 2022GY-193.

Data Availability Statement: The data supporting the results of this study was obtained from the NASA Prognostics Center of Excellence (PCoE). Available online: https://ti.arc.nasa.gov/tech/dash/groups/pcoe/prognostic-data-repository (accessed on 15 July 2022).

Conflicts of Interest: The authors declare no conflict of interest.

References

1. Ghorbanzadeh, M.; Astaneh, M.; Golzar, F. Long-term degradation based analysis for lithium-ion batteries in off-grid wind-battery renewable energy systems. *Energy* **2019**, *166*, 1194–1206. [CrossRef]
2. Xu, J.L.; Liu, B.L.; Zhang, G.Y.; Zhu, J.W. State-of-health estimation for lithium-ion batteries based on partial charging segment and stacking model fusion. *Energy Sci. Eng.* **2023**, *11*, 383–397. [CrossRef]
3. Li, J.; Li, Y.; Chen, G.; Lyu, C.; Wu, Y.; Xu, L.; Ma, S. Research on Feature Extraction and SOH Evaluation Methods for Retired Power Battery. *Proc. Chin. Soc. Electr. Eng.* **2022**, *42*, 1332–1346.
4. Pang, B.; Chen, L.; Dong, Z.M. Data-Driven Degradation Modeling and SOH Prediction of Li-Ion Batteries. *Energies* **2022**, *15*, 5580. [CrossRef]
5. Shen, S.Q.; Liu, B.C.; Zhang, K.; Ci, S. Toward Fast and Accurate SOH Prediction for Lithium-Ion Batteries. *IEEE Trans. Energy Convers.* **2021**, *36*, 2036–2046. [CrossRef]
6. Chen, D.; Meng, J.H.; Huang, H.Y.; Wu, J.; Liu, P.; Lu, J.W.; Liu, T.Q. An Empirical-Data Hybrid Driven Approach for Remaining Useful Life prediction of lithium-ion batteries considering capacity diving. *Energy* **2022**, *245*, 12. [CrossRef]
7. Iurilli, P.; Brivio, C.; Carrillo, R.E.; Wood, V. Physics-Based SoH Estimation for Li-Ion Cells. *Batteries* **2022**, *8*, 204. [CrossRef]
8. Wen, J.C.; Zou, Q.R.; Chen, C.G.; Wei, Y.J. Linear correlation between state-of-health and incremental state-of-charge in Li-ion batteries and its application to SoH evaluation. *Electrochim. Acta* **2022**, *434*, 10. [CrossRef]

9. Wu, T.Z.; Liu, S.Z.; Wang, Z.K.; Huang, Y.H. SOC and SOH Joint Estimation of Lithium-Ion Battery Based on Improved Particle Filter Algorithm. *J. Electr. Eng. Technol.* **2022**, *17*, 307–317. [CrossRef]
10. Sun, S.; Sun, J.Z.; Wang, Z.L.; Zhou, Z.Y.; Cai, W. Prediction of Battery SOH by CNN-BiLSTM Network Fused with Attention Mechanism. *Energies* **2022**, *15*, 4428. [CrossRef]
11. Li, Q.; Zhang, X.; Zhao, K.; Sun, J.; Wang, K. State of Health Estimation of Lithium-ion Battery Based on Ant Lion Optimization and Support Vector Regression. In Proceedings of the 2021 IEEE International Conference on Electrical Engineering and Mechatronics Technology (ICEEMT), Qingdao, China, 2–4 July 2021; pp. 334–337.
12. Wang, Y.; Ni, Y.; Zheng, Y.; Shi, X.; Wang, J. Remaining Useful Life Prediction of Lithium-ion Batteries Based on Support Vector Regression Optimized and Ant Lion Optimizations. *Proc. Chin. Soc. Electr. Eng.* **2021**, *41*, 1445–1457.
13. Xu, J.; Ni, Y.; Zhu, C. Remaining Useful Life Prediction for Lithium-Ion Batteries Based on Improved Support Vector Regression. *Trans. China Electrotech. Soc.* **2021**, *36*, 3693–3704.
14. Ye, J.Y.; Yang, Z.X.; Li, Z.L. Quadratic hyper-surface kernel-free least squares support vector regression. *Intell. Data Anal.* **2021**, *25*, 265–281. [CrossRef]
15. Cheng, Y.; Zheng, L.; Liu, J. Lithium battery health state estimation based on mode decomposition and time series. *J. Power Supply* **2023**. Available online: https://kns.cnki.net/kcms/detail/12.1420.TM.20230131.1102.001.html (accessed on 21 February 2023).
16. Khumprom, P.; Yodo, N. A Data-Driven Predictive Prognostic Model for Lithium-ion Batteries based on a Deep Learning Algorithm. *Energies* **2019**, *12*, 660. [CrossRef]
17. Xu, Z.Y.; Guo, Y.J.; Saleh, J.H. A physics-informed dynamic deep autoencoder for accurate state-of-health prediction of lithium-ion battery. *Neural Comput. Appl.* **2022**, *34*, 15997–16017. [CrossRef]
18. Hu, X.; Guo, Y.; Zhang, R. Review of State-of-health Estimation Methods for Lithium-ion Battery. *J. Power Supply* **2022**, *20*, 126–133.
19. Meng, J.H.; Cai, L.; Stroe, D.I.; Huang, X.R.; Peng, J.C.; Liu, T.Q.; Teodorescu, R. An Automatic Weak Learner Formulation for Lithium-Ion Battery State of Health Estimation. *IEEE Trans. Ind. Electron.* **2022**, *69*, 2659–2668. [CrossRef]
20. Zhang, C.; Zhao, S.; He, Y. State-of-health Estimate for Lithium-ion Battery Using Information Entropy and PSO-LSTM. *J. Mech. Eng.* **2022**, *58*, 180–190.
21. Zhang, Y.N.; Lian, Z.; Fu, W.L.; Chen, X. An ESR Quasi-Online Identification Method for the Fractional-Order Capacitor of Forward Converters Based on Variational Mode Decomposition. *IEEE Trans. Power Electron.* **2022**, *37*, 3685–3690. [CrossRef]
22. Ding, G.R.; Wang, W.B.; Zhu, T. Remaining Useful Life Prediction for Lithium-Ion Batteries Based on CS-VMD and GRU. *IEEE Access* **2022**, *10*, 89402–89413. [CrossRef]
23. Xue, J.K.; Shen, B. Dung beetle optimizer: A new meta-heuristic algorithm for global optimization. *J. Supercomput.* **2022**, *79*, 7305–7336. [CrossRef]
24. Wei, R.; Mao, T.; Gao, H.; Peng, J.; Yang, J. Health state estimation of lithium ion battery based on TWP-SVR. *Energy Storage Sci. Technol.* **2022**, *11*, 2585–2599.
25. Zhou, X.; Li, N.; Pan, Y.; Sun, L. Optimized SVR based on artificial bee colony algorithm for leaf area index inversion. *J. Remote Sens.* **2022**, *26*, 766–780.
26. Zhou, S.; Yang, C.C.; Su, Z.N.; Yu, P.; Jiao, J. An Aeromagnetic Compensation Algorithm Based on Radial Basis Function Artificial Neural Network. *Appl. Sci.* **2023**, *13*, 136. [CrossRef]
27. Huang, K.; Ding, H.; Guo, Y.; Tian, H. Prediction of Remaining Useful Life of Lithium-Ion Battery Based on Adaptive Data Preprocessing and Long Short-Term Memory Network. *Trans. China Electrotech. Soc.* **2022**, *37*, 3753–3766.